

Turbo-XAS: dispersive XAS using sequential acquisition

S. Pascarelli,* T. Neisius and S. De Panfilis

ESRF, BP 220, 38043 Grenoble, France. E-mail: sakura@esrf.fr

(Received 29 October 1998; accepted 23 March 1999)

A new experimental technique for time-resolved X-ray absorption studies in the sub-second range has been successfully tested on the dispersive XAS beamline (ID24) at the ESRF. It consists of a sequential acquisition of energy points using the dispersive optics scheme installed on the beamline. Turbo-XAS takes full advantage of the properties of third-generation radiation sources, overcoming many of the problems encountered in the classical dispersive XAS mode, based on position-sensitive detectors. The new technique benefits from the basic assets of the dispersive set-up, *i.e.* the absence of movement of the optics and the extremely small and stable horizontal focal spot. In addition, it features simultaneous recording of I_0 and I_1 and the possibility of performing fluorescence and electron detection.

Keywords: X-ray absorption spectroscopy (XAS); time-resolved XAS; energy-dispersive optics.

1. Introduction

Time-resolved X-ray absorption spectroscopy using energy-dispersive optics has shown in the past 15 years to be an invaluable tool in the investigation of the electronic and local structure in condensed matter during dynamical processes. Moreover, thanks to the absence of movement of the optics and to the small and stable horizontal focal spot, the dispersive set-up has proved to have unique characteristics for the study of small samples in restrictive environmental cells as well as for the detection of very small signals, like those encountered in X-ray magnetic circular dichroism.

Starting from the pioneering work of Matsushita *et al.* (Matsushita & Kaminaga, 1980), the parallel energy acquisition mode (dispersive mode, or D-XAS) has been further developed at the different synchrotron radiation facilities (Phizackerley *et al.*, 1983; Flank *et al.*, 1983; Allinson *et al.*, 1988; Hagelstein *et al.*, 1989; D'Acapito *et al.*, 1992; Allen *et al.*, 1992; Lee *et al.*, 1994) and extensively exploited in different scientific domains, from chemistry to biology to solid-state physics (for a review see Fontaine *et al.*, 1989, and references therein).

The dispersive XAS beamline at the ESRF (Hagelstein *et al.*, 1997) has been specifically designed to benefit from the high brilliance of its undulator source, in order to reach a time resolution in the sub-millisecond range. A position-sensitive detector (PSD), consisting of a scintillator screen coupled to a CCD camera with a fast analog buffer, has been designed in order to reach such a time resolution (Koch *et al.*, 1996). Thanks to the high flux available, both Bragg and Laue geometries (Hagelstein *et al.*, 1995; San Miguel *et al.*, 1998) for the polychromator crystal can be used, in order to cover the entire energy range from 5 to 27 keV with an optimized energy resolution.

Recently, a new design for the polychromator crystal has lead to an aberration-free horizontal focal spot (Pellicer Porres, San Miguel & Fontaine, 1998) of $\sim 20 \mu\text{m}$ FWHM in a large energy range, opening unique possibilities for performing X-ray absorption studies under extreme conditions of temperature and pressure (Itié *et al.*, 1997; San Miguel *et al.*, 1998; Pellicer Porres, Segura *et al.*, 1998). Moreover, the implementation of quarter-wave plates on dispersive set-ups (Giles *et al.*, 1994) has allowed the recording of extremely accurate XMCD spectra (Pizzini *et al.*, 1998). Very recently the single-bunch filling mode of the machine at the ESRF has been combined with a microcoil to generate a pulsed magnetic field pump phased with respect to the probe to study nanosecond-resolved dispersive XMCD (Bonfim *et al.*, 1998).

These examples show that the advent of third-generation sources has certainly given a new perspective to the field of time-resolved X-ray absorption in the dispersive mode. However, the reduction of source size, the lengthening of beamlines (due to the increase in machine diameters), as well as the increased power load on the optics, have introduced new problems related to the much higher sensitivity to beam instabilities (Pascarelli *et al.*, 1999). With respect to the conventional scanning mode, the dispersive set-up is intrinsically more sensitive to such instabilities. In fact, up to now, no successful attempt to record simultaneously the intensity before (I_0) and after (I_1) the sample using a parallel acquisition mode has been made, leading to normalization problems in the case of beam instabilities. Moreover, as the spectra are obtained by conversion of a one-dimensional image, they suffer from distortions due to phase contrast phenomena associated with imperfections in all elements in the beam path, and to small-angle scattering from the sample, which strongly affect the quality of the data,

particularly on powder samples (Hagelstein *et al.*, 1997, 1998).

Time-resolved X-ray absorption in the sequential mode, using a fast-scanning double-crystal monochromator (Frahm, 1988, 1989; Als-Nielsen *et al.*, 1995) or a piezo-driven vibrating double-crystal monochromator (Bornebusch *et al.*, 1999), leads to a set-up with an intrinsic lower sensitivity to beam instabilities, due to the simultaneous recording of I_0 and I_1 . Also, sequential acquisition enables detection of decay channels, thereby opening the way to time-resolved investigations of the changes in the structure or valence states of a wide variety of samples which are inaccessible for transmission spectroscopy. The time resolution, the position stability of the focal spot and the stability of the energy scale in such methods are, however, limited by the mechanical movement of the two crystals.

We have recently successfully tested on ID24 a new experimental set-up which allows a very good time resolution to be maintained, while offering a correct normalization due to the simultaneous recording of I_0 and I_1 . In turbo-XAS (T-XAS), absorption spectra are recorded using two gas detectors or photodiodes, positioned before

and after the focal point, respectively, which measure the signal generated by a monochromatic beam, obtained by scanning a narrow slit through the energy-dispersed fan of radiation immediately after the polychromator. This technique is successful at the ESRF thanks to the small source size, which allows energy resolution to be controlled by the width of the slit.

The simultaneous recording of I_0 and I_1 is the essential new feature with respect to D-XAS, leading to an experimental set-up which is intrinsically less sensitive to beam instabilities. A good time resolution is maintained, as preliminary XAS spectra have been recorded on timescales of 0.05 (XANES) to 0.5 s (EXAFS). The experimental set-up also profits from the small and stable horizontal focal point and high energy scale stability and reproducibility of the dispersive optics thanks to the decoupling of the monochromatization and of the focusing action. Finally, T-XAS enables detection of decay channels, opening the way to time-resolved studies of surfaces and dilute samples using dispersive optics.

The main applications of the new technique envisaged on ID24 are in the field of dynamical processes on the second

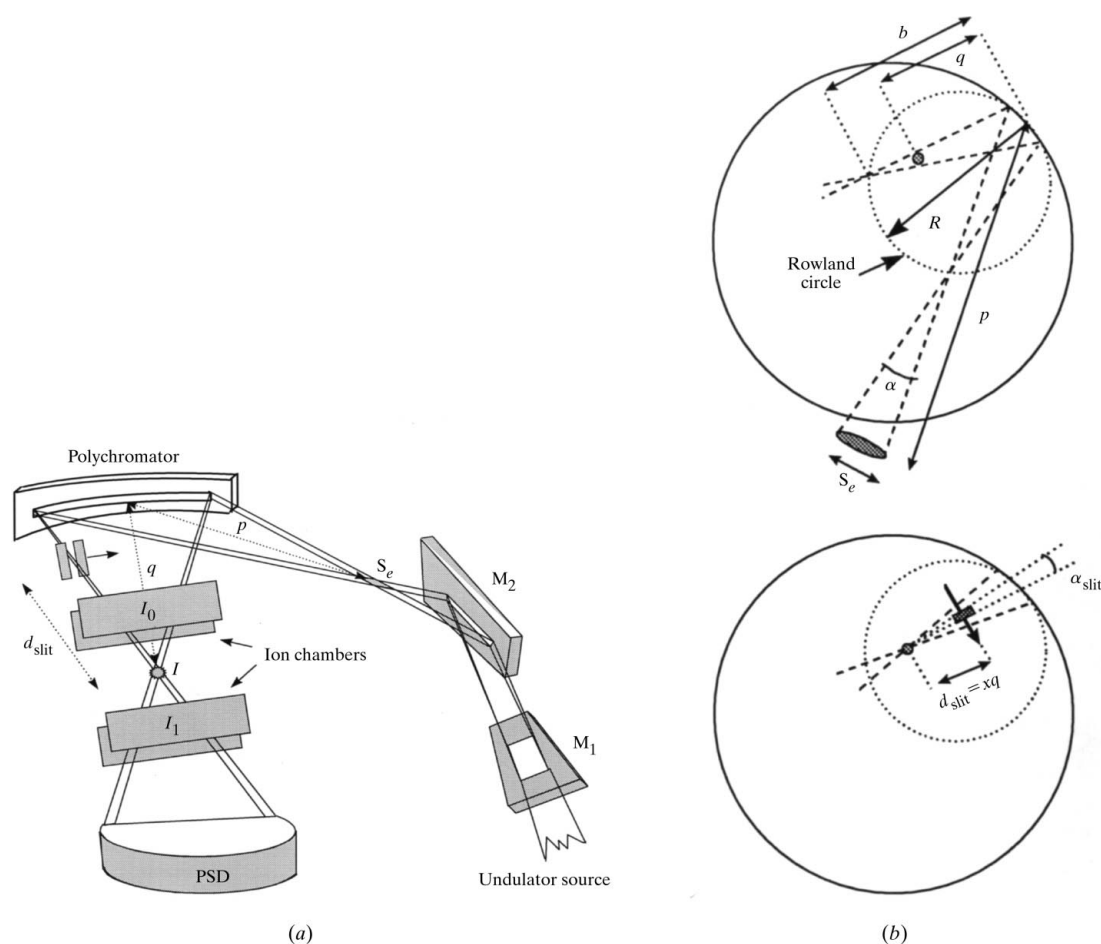


Figure 1

(a) Optical layout of beamline ID24 and experimental set-up for T-XAS. A narrow slit is scanned through the polychromatic fan of radiation downstream of the crystal, selecting a monochromatic beam, the intensity of which is simultaneously recorded before and after the sample by two ionization chambers. (b) The contributions due to source size, S_e , and slit size, σ , to the calculation of the angular spread in Bragg angle, $\delta\theta$, on the crystal.

timescale, mainly in the transmission mode but also using the reflection mode or fluorescence/electron yield detection. Due to the possibility of obtaining a correct normalization of the data, T-XAS will also be widely employed for the large number of static XAS experiments which need dispersive optics because of the small and stable focal spot, such as high-pressure experiments (Itié *et al.*, 1997; Pellicer Porres, Segura *et al.*, 1998) and micro-XANES (Mosbah *et al.*, 1998), or which need a high stability of the energy scale, such as XMCD measurements (Pizzini *et al.*, 1998; Bonfim *et al.*, 1998).

2. Experimental

Fig. 1(a) shows a schematic diagram of the optics layout of beamline ID24, as well as the experimental set-up required for T-XAS. The beamline is installed on an undulator source on a high-beta section of the ring, and operates in the energy range 5–27 keV. The first mirror (M_1) focuses the beam in the vertical plane at the sample position while the second mirror (M_2) has the double action of demagnifying the horizontal source and of opening a ~ 1 mrad horizontally diverging fan of radiation which impinges on the curved crystal. The crystal is positioned on the θ axis of a θ - 2θ spectrometer, with the PSD lying at the extreme of the 2θ axis.

The radius of curvature of the crystal is obtained by the well known relationship of cylindrical optics,

$$1/p + 1/q = 2/R \sin \theta, \quad (1)$$

where R is the crystal radius, θ is the Bragg angle, and p and q are defined in Fig. 1(a). The change of the Bragg angle along the surface of the crystal, $\Delta\theta$, opens an energy bandpass, ΔE , given by

$$\Delta E = E \cot \theta \Delta\theta = E \cot \theta (Pl \sin \theta), \quad (2)$$

where l is the illuminated length of the crystal and P is defined as

$$P = 1/R \sin \theta - 1/p. \quad (3)$$

The crystal yields a polychromatic focus point, I , at a distance q from the crystal (typically 1–2 m), which is the image of the effective source, S_e , at a distance from the crystal of $p \simeq 30$ m. I is the optimal position for the sample. In the standard dispersive set-up (D-XAS), the PSD converts the ‘energy–direction’ correlation into ‘energy–position’ correlation, and allows for parallel recording of the entire absorption spectrum in the energy interval ΔE , in the form of a one-dimensional image.

In T-XAS, a narrow (~ 30 – 50 μm) slit is scanned through the polychromatic fan of radiation downstream of the crystal, selecting a monochromatic beam, the intensity of which is simultaneously recorded before and after the sample by two ionization chambers, as shown in Fig. 1(a). The slit, of width σ , is located at a distance from the sample $d_{\text{slit}} = xq$ ($0 < x < 1$). Energy resolution is determined, as in D-XAS, by four factors: the crystal diffracting planes

(which determine the intrinsic energy resolution), the dimensions of the slit (or of the PSD pixels in D-XAS), the source horizontal dimensions, and the crystal penetration depth.

Preliminary tests were directed at first in establishing the adequacy of such a concept, the main concern being the effects of source size on energy resolution.

It is well known (Tolentino *et al.*, 1988) that in D-XAS the contribution to energy resolution due to a finite source size can be minimized by placing the PSD on or close to the Rowland circle of energy E at a distance $b = R \sin \theta$ from the crystal (see Fig. 1b). Note that $b \simeq P^{-1}$ whenever $p \gg q$, as is the case on ID24 [see equation (3)].

In T-XAS the source size contribution cannot be minimized using this method and can effectively be the limiting

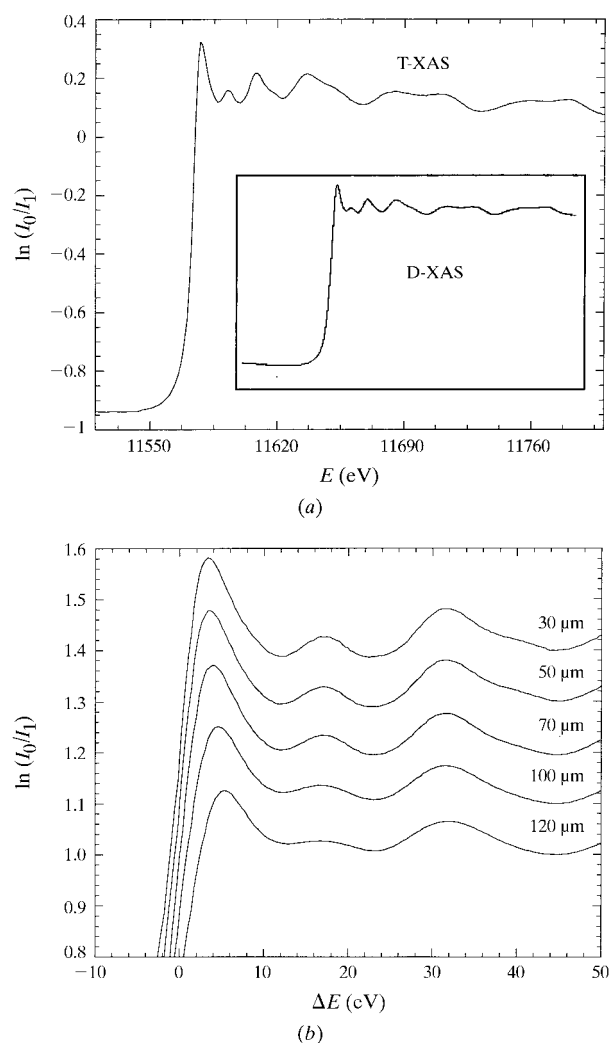
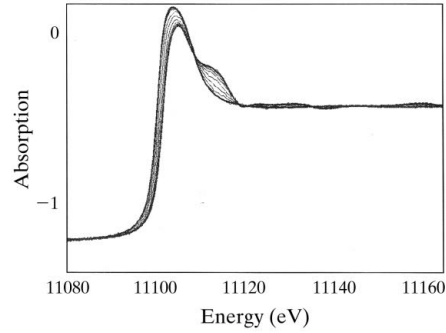
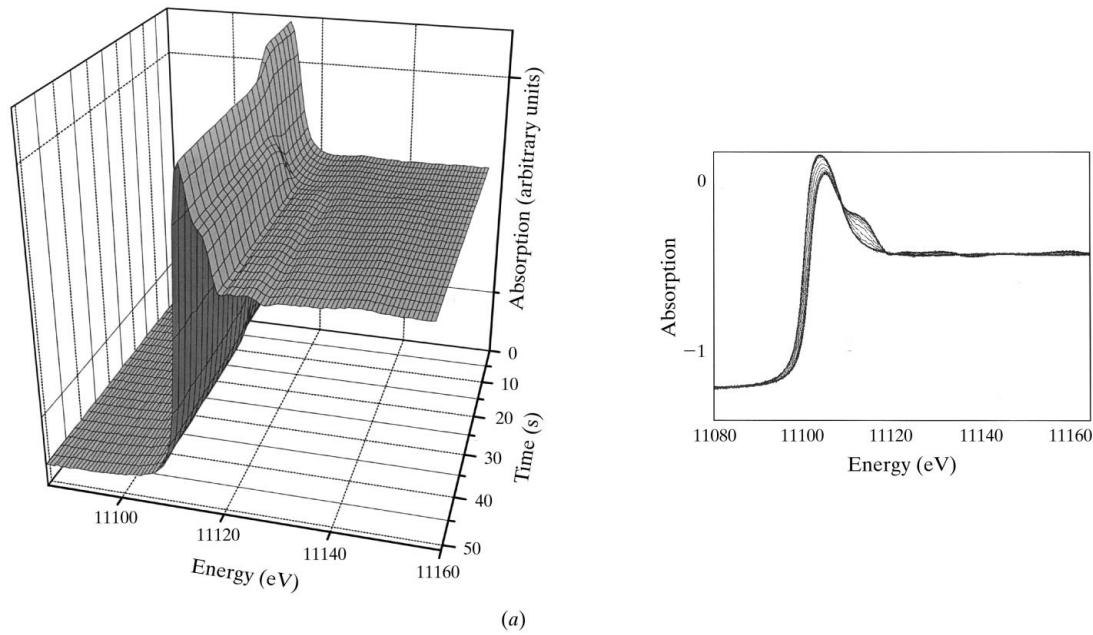


Figure 2
(a) Pt L_{III} EXAFS recorded using T-XAS. The slit dimensions and position were $\sigma = 30$ μm and $x = 0.5$. The inset shows the same spectrum recorded using the CCD camera (D-XAS), indicating that energy resolution is comparable. (b) Pt L_{III} XANES recorded using $x = 0.5$ and $\sigma = 30, 50, 70, 100$ and 120 μm . Degradation in energy resolution is visible for $\sigma > 50$ μm , in agreement with equation (4).

**Figure 3**

(a) Sequence of Ge *K*-edge XANES spectra recorded in 120 ms spectrum⁻¹ during a rapid cooling from the melt: the metal–semiconductor transition appears at ~350 K below the melting point, with the absorption edge gradually shifting towards higher energies, indicative of the formation of the gap. (b) Sequence of Ge *K*-edge EXAFS spectra recorded in 520 ms spectrum⁻¹ during a rapid cooling. The initial temperature is 1115 K, while the final temperature is 732 K. The temperature variation is not linear with time.

factor to energy resolution. In fact, the total angular spread in Bragg angle, $\delta\theta$, relative to the portion of the fan selected by the slit is given by

$$\delta\theta = \delta\theta_{\text{slit}} + \delta\theta_{\text{source}},$$

where $\delta\theta_{\text{slit}}$ and $\delta\theta_{\text{source}}$ are the angular spreads in Bragg angle related to the width of the slit and to the source size, respectively (see Appendix A),

$$\delta\theta_{\text{slit}} = (\sigma/x)P$$

and

$$\delta\theta_{\text{source}} = \alpha bP \simeq \alpha.$$

α is the fan of rays emitted by the source of size S_e and impinging on the crystal at the same Bragg angle,

$$\alpha = S_e/(p - b).$$

On ID24, $\alpha \simeq 7 \mu\text{rad}$ and the contribution $\delta\theta_{\text{source}}$ is always smaller than the intrinsic angular acceptance (Ω_{111}) of the Si(111) crystal[†] thanks to the small size ($S_e \simeq 200 \mu\text{m}$) of the effective source.

In order to have $\delta\theta \simeq \Omega$, the following condition on the ratio σ/x must be respected,

$$\sigma/x = \Omega P^{-1}. \quad (4)$$

[†] This is true for Si(311) crystals up to a maximum energy of 16 keV.

3. Results

Preliminary tests have been performed at the K -edges of Fe, Cu, Ga, Ge and Zr and at the L_{III} -edges of Pt and Au using Si(111) and Si(311) crystals in the Bragg geometry. The photon flux measured on the sample through the slit was $\sim 10^9$ photons s^{-1} . The current generated in the N_2 - or Ar-filled ion chambers was of the order of 10^{-7} – 10^{-9} A. Different signal-processing methods were tested. In all cases the current generated by the ion chambers was amplified by fast current amplifiers. The output signal was then either converted by a 1 MHz voltage-to-frequency converter or by a 16 bit ADC. The acquisition of the I_0 and I_1 signals is performed simultaneously at constant time intervals Δt while the slit is continuously scanned through the beam. Using the ADC it was possible to use $\Delta t = 400$ μs and to record good quality XANES and EXAFS spectra in ~ 50 and 500 ms, respectively.

3.1. Energy resolution

The first tests were directed at investigating the achievable energy resolution using this new concept. We have observed that energy resolution can be effectively controlled by varying the width, σ , of the slit. Fig. 2(a) shows a comparison of the Pt L_{III} EXAFS recorded with an Si(111) crystal using T-XAS and D-XAS (inset). The slit width was $\sigma = 30$ μm while $x = 0.5$. Energy resolution is indeed comparable in the two set-ups. Fig. 2(b) compares Pt L_{III} XANES recorded with $\sigma = 30, 50, 70, 100$ and 120 μm . Degradation in energy resolution is visible for $\sigma > 50$ μm , in agreement with equation (4), where $\Omega \simeq 25$ μrad and $P^{-1} \simeq b \simeq 2.85$ m.

3.2. Time resolution

Fig. 3 illustrates results on one of the first applications of T-XAS. This experiment was aimed at providing insight into the evolution of a supercooled liquid as a function of

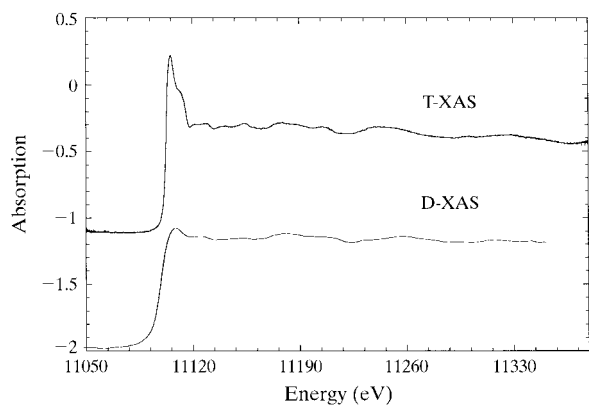


Figure 4

Effect of SAXS from powders on D-XAS spectra. The figure shows a comparison between a T-XAS and a D-XAS Ge K -edge spectra on a powder Ge sample in a BN matrix: the effect of energy-resolution degradation is apparent in the much lower intensity of the Ge K -edge white line on the D-XAS spectrum.

temperature. Taking advantage of the sub-second time resolution, snapshots of the electronic and local atomic structure of undercooled Ge melt have been taken before and during the appearance of the crystallites. Such an investigation is of fundamental interest due to the interplay between the covalent and metallic character of the bonding which characterize the solid and liquid phases of Ge, respectively. Pure Ge was chosen as a model sample; however, this experiment opens the way to the study of the electronic and local structure in metastable phases in

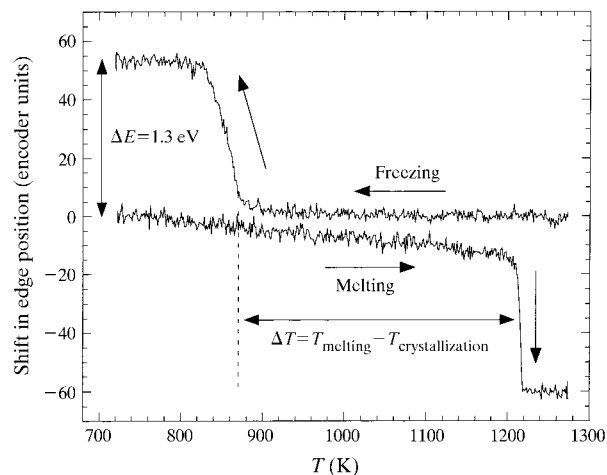


Figure 5

Plotted as a function of sample temperature are the backlash-corrected encoder positions corresponding to the onset of the Ge K -edge relative to 500 spectra (two-way scans), during a cooling and a melting cycle. The edge shift of approximately 55 encoder units (equivalent to ~ 1.3 eV) at the melting and freezing temperatures are evident. The position reproducibility is about ± 3 encoder units, corresponding to $\delta E \simeq \pm 0.07$ eV at 11.1 keV.

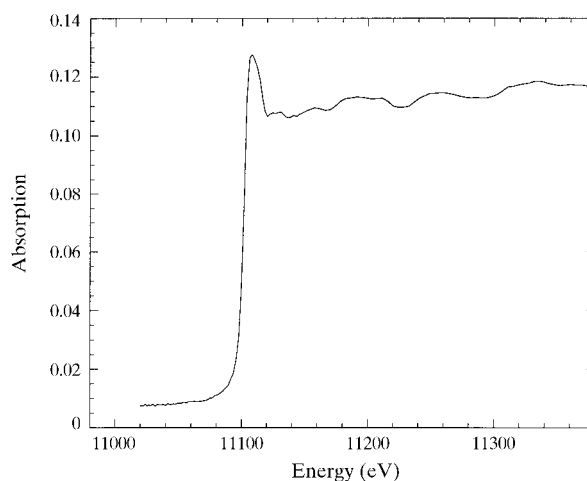


Figure 6

To demonstrate the possibilities in studying dilute samples, a Ge K -edge EXAFS spectrum on a test sample containing 1 wt% of the same Ge powder in a BN matrix is shown. Clearly, self-absorption effects are present, due to the nature of the sample (pure Ge powder of average grain size ~ 1 μm). The total acquisition time is 2 s.

semiconductor and metallic alloys. Polycrystalline Ge in powder form was heated to the melting point and then cooled down at different rates in order to observe the supercooled phase. The XANES spectra (Fig. 3*a*) clearly show a gradual shift towards higher energies and a strong attenuation of the white line, indicating the onset of the liquid metal–semiconductor transition, while the modifications in the EXAFS oscillations (Fig. 3*b*) mark the onset of the reconstruction of the tetrahedral network with the formation of crystallites. Such an experiment has also been carried out using D-XAS; however, due to the strong SAXS from the powder particles, which degrades energy resolution (see Fig. 4), all the fine structure features are broadened.

3.3. Dead time between scans

Due to the nature of the movement of the slit, which has to return to the initial position in between scans, the dead time between spectra is approximately 800 ms. By recording scans also during the return trip (two-way scan acquisition), this dead time can be reduced slightly, but not eliminated due to the fact that the slit must stop before inverting its direction. This drawback will be eliminated in the near future by using a rotating disc with an engraved spiral. One revolution of the disc swipes the slit once through the radiation fan. This solution also eliminates the need of backlash corrections.

3.4. Reproducibility in slit position/energy

If two-way scans are recorded, a backlash correction of about 10 encoder units† has to be performed on the encoder position of every second scan. After removing this quantity from every second scan, the overall position reproducibility is ± 3 encoder units, which corresponds to $\delta E \simeq \pm 0.07$ eV at 11.1 keV (see Fig. 5). This δE is about one order of magnitude smaller than the global energy resolution.

3.5. Restored sensitivity to dilute samples

Tests were also devoted to assess the feasibility of fluorescence detection on dilute samples. Fig. 6 illustrates an example of the possibilities in the study of dilute samples. It shows a Ge *K*-edge EXAFS spectra on a test sample containing 1 wt% of the same Ge powder in a BN matrix, recorded in 2 s. Clearly, self-absorption effects are present, due to the nature of the sample (pure Ge powder of average grain size ~ 1 μm). The fluorescence yield was measured using an unbiased Si photodiode in the current mode. Due to the relatively low concentration, the measurement in the transmission mode using the CCD camera is prohibitive on this sample.

† The exact value depends on the chosen speed and acceleration parameters of the motion of the slit.

4. Conclusions

A new simple method of recording time-resolved X-ray absorption spectra has been successfully tested. T-XAS features the basic assets of dispersive XAS, namely the absence of movement of the optics during data acquisition, leading to a high stability in energy scale and focal spot size and position. It also allows for simultaneous acquisition of the incident and transmitted intensity, yielding correct normalization of data, while maintaining a sub-second time resolution. In no way can T-XAS compete with D-XAS concerning time resolution: T-XAS and D-XAS are therefore complementary. This is illustrated with different examples, and lies primarily in the possibility of T-XAS to detect decay channels and to investigate powder samples. T-XAS therefore opens the way to time-resolved investigations of the changes in the structure or valence states of a wide variety of samples which are inaccessible for energy-dispersive spectroscopy in the transmission mode.

APPENDIX A

The total spread in Bragg angle, $\delta\theta$, relative to a divergent beam impinging on a curved crystal is given by

$$\delta\theta = wP,$$

where w is the width of the incident fan on the crystal and P is defined in equation (3). From Fig. 1(*b*),

$$w_{\text{slit}} = \alpha_{\text{slit}}q = (\sigma/xq)q = \sigma/x$$

and

$$w_{\text{source}} = \alpha b.$$

Therefore,

$$\delta\theta_{\text{slit}} = (\sigma/x)P$$

and

$$\delta\theta_{\text{source}} = \alpha bP.$$

References

- Allen, P. G., Conradson, S. D. & Penner-Hahn, J. E. (1992). *Synchrotron Rad. News*, **5**, 16–24.
- Allinson, N. M., Baker, G., Greaves, G. N. & Nicoll, K. J. (1988). *Nucl. Instrum. Methods*, **A266**, 592–597.
- Als-Nielsen, J., Grubel, G. & Clausen, B. S. (1995). *Nucl. Instrum. Methods Phys. Res. B*, **97**, 522–525.
- Bonfim, M., Mackay, K., Pizzini, S., San Miguel, A., Tolentino, H., Giles, C., Neisius, T., Hagelstein, M., Baudelet, F., Malgrange, C. & Fontaine, A. (1998). *J. Synchrotron Rad.* **5**, 750–752.
- Bornebusch, H., Clausen, B. S., Steffensen, G., Lutzenkirchen-Hecht, D. & Frahm, R. (1999). *J. Synchrotron Rad.* **6**, 209–211.
- D'Acapito, F., Boscherini, F., Marcelli, A. & Mobilio, S. (1992). *Rev. Sci. Instrum.* **63**, 899–901.
- Flank, A. M., Fontaine, A., Jucha, A., Lemonnier, M., Raoux, D. & Williams, C. (1983). *Nucl. Instrum. Methods*, **208**, 651–654.
- Fontaine, A., Dartyge, E., Itie, J. P., Polian, A., Tolentino, H. & Tourillon, G. (1989). *Topics in Current Chemistry 151*, pp. 180–203. Berlin: Springer.
- Frahm, R. (1988). *Nucl. Instrum. Methods*, **A270**, 578–581.

- Frahm, R. (1989). *Rev. Sci. Instrum.* **60**, 2515–2518.
- Giles, C., Malgrange, C., Goulon, J., de Bergevin, F., Vettier, C., Dartyge, E., Fontaine, A., Giorgetti, C. & Pizzini, S. (1994). *J. Appl. Cryst.* **27**, 232–240.
- Hagelstein, M., Cunis, S., Frahm, R., Niemann, W. & Rabe, P. (1989). *Physica B*, **158**, 324–325.
- Hagelstein, M., Ferrero, C., Hatje, U., Ressler, T. & Metz, W. (1995). *J. Synchrotron Rad.* **2**, 174–180.
- Hagelstein, M., Lienert, U., Ressler, T., San Miguel, A., Freund, A., Cunis, S., Schulze, C., Fontaine, A. & Hodeau, J. L. (1998). *J. Synchrotron Rad.* **5**, 753–755.
- Hagelstein, M., San Miguel, A., Fontaine, A. & Goulon, J. (1997). *J. Phys. IV*, **7**, 303–308.
- Itié, J. P., Gauthier, M., Polian, A. & San Miguel, A. (1997). *ESRF Highlights 1996/97*. ESRF, Grenoble, France.
- Koch, M., Hagelstein, M., San Miguel, A., Fontaine, A. & Ressler, T. (1996). *Proc. SPIE*, **2416**, 85–93.
- Lee, P. L., Beno, M. A., Jennings, G., Ramanathan, M., Knapp, G. S., Huang, K., Bai, J. & Montano, P. A. (1994). *Rev. Sci. Instrum.* **65**, 1–6.
- Matsushita, T. & Kaminaga, U. (1980). *Jpn. J. Appl. Cryst.* **13**, 465–472.
- Mosbah, M., Metrich, N., Duraud, J. P., San Miguel, A., Delaney, J. S. & McCammon, C. (1998). *Exp. Mineral. Petrol. Geochem. VII Int.*, April 1998, Orleans, France.
- Pascarelli, S., Neisius, T., De Panfilis, S., Bonfim, M., Pizzini, S., Mackay, K., David, S., Fontaine, A., San Miguel, A., Itié, J. P., Gauthier, M. & Polian, A. (1999). *J. Synchrotron Rad.* **6**, 146–148.
- Pellicer Porres, J., San Miguel, A. & Fontaine, A. (1998). *J. Synchrotron Rad.* **5**, 1250–1257.
- Pellicer Porres, J., Segura, A., San Miguel, A. & Munoz, V. (1998). *Phys. Status Solidi*, **B211**, 389–393.
- Phizackerley, R. P., Rek, Z. U., Stephenson, G. B., Conradson, S. D., Hodgson, K. O., Matsushita, T. & Oyanagi, H. (1983). *J. Appl. Cryst.* **16**, 220–232.
- Pizzini, S., Bonfim, M., Baudalet, F., Tolentino, H., San Miguel, A., MacKay, K., Malgrange, C., Hagelstein, M. & Fontaine, A. (1998). *J. Synchrotron Rad.* **5**, 1298–1303.
- San Miguel, A., Hagelstein, M., Borrel, J., Marot, G. & Renier, M. (1998). *J. Synchrotron Rad.* **5**, 1396–1397.
- Tolentino, H., Dartyge, E., Fontaine, A. & Tourillon, G. (1988). *J. Appl. Cryst.* **21**, 15–21.